THE JOURNAL OF PHYSICAL CHEMISTRY C

Article

Cite This: J. Phys. Chem. C 2019, 123, 16153−16163

pubs.acs.org/JPCC

Water Redistribution−Microdiffusion in Cement Paste under Mechanical Loading Evidenced by ^{1}H NMR

Mateusz Wyrzykowski,*[,†] Agata M. Gajewicz-Jaromin,[‡] Peter J. McDonald,[‡] David J. Dunstan,[§] Karen L. Scrivener,[∥] and Pietro Lura[†,⊥]

[†]Concrete and Construction Chemistry Laboratory, Empa, Swiss Federal Laboratories for Materials Science and Technology, 8600 Dübendorf, Switzerland

[‡]Department of Physics, University of Surrey, Guildford, Surrey GU2 7XH, U.K.

[§]School of Physics and Astronomy, Queen Mary University of London, London E1 4NS, U.K.

[∥]Laboratory of Construction Materials, EPFL, 1015 Lausanne, Switzerland

[⊥]Institute for Building Materials, ETH Zurich, 8093 Zurich, Switzerland

Supporting Information

ABSTRACT: The mobility of water within the microstructure of hardened cement paste has been at the center of a long-lasting debate, motivated by the need to understand the fundamental mechanisms that play a role in drying, shrinkage, creep, and thermal expansion. Our ^{1}H NMR results show for the first time that externally applied pressure can lead to migration of water within the microstructure (microdiffusion). Upon compression, the gel water signal decreases. For the most part, this is accommodated by a corresponding increase in the signal of water in larger, interhydrate, and capillary spaces. However, there is also an increase in the signal corresponding to the water in most confined spaces. Normally, such tiny spaces are classified as hydrate interlayers. However, we do not conclude that there is a significant increase in interlayer water. Rather, we attribute this part of the increase to a rearrangement of the microstructure upon compression with some water confined in increasingly small gel pore spaces. These findings show that the deformability of the microstructure (C−S−H gel) at the expense of gel porosity may explain part of the macroscopic deformations due to short-term creep.

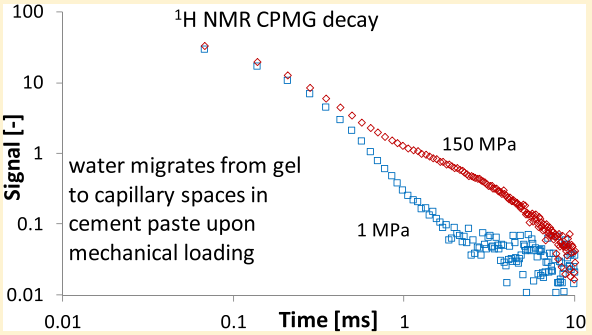

1. INTRODUCTION

Hardened cement paste is composed of different hydration products, unhydrated cement (or, more generally, binder, including also fillers or supplementary cementitious materials—SCM), and porosity. The small pores in the cement paste, with their high specific surface area, are responsible for the strong interactions of cement paste with different fluids (pore fluid, water vapor, liquid water, and other fluids or gases that can penetrate from the outside).[1−3] These interactions further govern such important phenomena as shrinkage, creep, and thermal deformation of cement-based materials like mortar or concrete.[2,4,5] In this regard, the porosity and the water within the calcium silicate hydrate (C−S−H), the main hydration product of Portland cement characterized by its very high specific surface, are especially important. Although the proposed sizes of spaces in which water is confined can vary depending on the experimental method and theoretical models of the microstructure of a hardened cement gel, a general classification is mostly agreed upon. The smallest spaces in which water is present as an intrinsic part of the hydration products are the C−S−H interlayer spaces (also referred to as the intra-C−S−H sheet pores[6]) between the backbone C−S−H sheets. Above the scale of the C−S−H sheets, water is present in the gel pores that form between the agglomerates of the C−S−H sheets and are an intrinsic part of the C−S−H gel.[3] Larger pores are present between the needles or globule flocks (depending on the adopted microstructural model) of C−S−H and are referred to as the interhydrate pores. Finally, capillary pores are formed as spaces from which water is consumed in the hydration process and consequently they are not filled with hydration products.[1,6,7] The nomenclature used in the cement research field will be used in this paper. Please refer to Table 1 for the summary of pores/spaces in cement paste and their sizes found in previous studies.

Already in the 1960s, Powers referred to water adsorbed in the narrowest spaces between solid hydrates, where the full adsorption thickness cannot develop, as the "hindered adsorption water".[15] According to recent experimental data obtained with ^{1}H nuclear magnetic resonance (NMR), these

Received: March 14, 2019
Revised: May 30, 2019
Published: June 7, 2019

Table 1. Classification of Water-Filled Spaces and Pores in Hydrated Cement Paste According to Different Sources

pore/space populations	description	characteristic sizes	IUPAC classification[8]
interlayer C−S−H spaces	spaces between the backbone C−S−H sheets	≤1 nm[9−12]	micropores
		1.5 nm[6]	
		1.8 nm[13]	
		<2 nm[14]	
gel pores	pores between the agglomerates (stacks or globules) of the C−S−H sheets, intrinsic part of the C−S−H gel	1−3 nm (small gel pores)[12]	mesopores
		3−12 nm (large gel pores between the globule flocks)[12]	
		2−3 nm[9,10]	
		7 nm[13]	
		2−8 nm[14]	
interhydrate pores	pores between the C−S−H needles	∼10 nm[9,10]	
		>8 nm[14]	
		50 nm[13]	
capillary pores	larger pores—remained after consumption of water	>8 nm[14]	macropores
		≥100 nm[9,10,13]	

spaces correspond to part of the interlayer water in the C−S−H and in small gel pores.[6,11] The hindered-adsorbed water was proposed by Powers to be subject to disjoining pressure (see also the works of Wittmann and co-workers[2,16]) and to act as load-bearing layers in the hydrated gel. Powers further suggested that creep deformations of cement paste are due to the transport of this water from the hindered adsorption areas to larger capillary pores in a diffusion process.[15,17] Such microdiffusion would be triggered when the equilibrium is upset locally by the application of external stress. According to this description, Powers proposed that creep is in fact "stress-induced shrinkage".[15] The concept of microdiffusion leading to stress-induced shrinkage was further studied within a thermodynamic framework by Bažant and co-workers.[18,19] A distinction between the volumetric short-term creep (days to few weeks) and deviatoric long-term creep has been observed experimentally in the previous studies.[20−22] Bernard et al.[21] measured the fast contraction of the samples under hydrostatic loading in very porous calcium-leached cement paste and mortar. This contraction was attributed to water movement. It is worth noting that the compaction of C−S−H (referred to as the "increase of the packing density") was observed also in nanoindentation tests.[23] Feldman[24] proposed that the "seepage" of adsorbed water from interlayer spaces could be responsible for short-term creep but should not be involved in long-term creep, for which shear slippage was proposed (see also the more recent micro-prestress theory of creep[25]). Microdiffusion as the mechanism responsible for short-term creep was later adopted in a number of models of concrete creep,[26−29] not least due to the ease of implementation in the viscoelastic models with dashpot elements corresponding to the diffusion process.

The microdiffusion process was proposed by Powers to account also for delayed thermal deformations since a temperature change would also cause a free energy potential between water in pores of different sizes.[17] This hypothesis was later adapted by Bažant and by Sellevold and Bjøentegaard.[30,31] In a recent study,[9] we observed immediate and reversible water redistribution from interlayer C−S−H spaces to gel pores during heating in the range of 20−38 °C.

The motivation of this study is to investigate experimentally whether water redistribution (microdiffusion) takes place due to mechanical loading and, if so, which populations of water are involved.

To this end, the state of the water in white Portland cement paste is measured by ^{1}H NMR T_2-relaxometry during the application of hydrostatic pressure (up to 150 MPa) in a pressure cell placed in an NMR magnet. ^{1}H NMR relaxometry is particularly useful for this purpose, thanks to the fact that it enables nondestructive in situ measurements with water itself (or, more precisely, hydrogen) in the cement paste acting as the probe.[13,32,33] Further, the measurements take advantage of the fact that the proton experiences different relaxation rates, which are proportional to the strength of interaction of the water with the solids.[6] This enables different populations of water to be distinguished in different classes of pore sizes (or chemophysically bound to solids in the case of the adsorbed or interlayer water) and water migration between them to be followed. ^{1}H NMR relaxometry has been recently used for studying the microstructure of C−S−H,[6,11,34] pore-size-resolved sorption isotherms,[10,35] hydration of cement,[36−38] kinetics of water migration in the microstructure during wetting,[39] self-desiccation,[40] self-healing of cracks,[41] drying,[42] moderate temperature changes,[9] or fire exposure.[43] The outcomes of many ^{1}H NMR experiments regarding porosity, sorption, and hydration process could be validated with independent experimental techniques, e.g., mercury intrusion porosimetry, X-ray diffractometry, or sorption isotherms.[10,44,45] However, to the best of our knowledge, no complementary experimental technique could directly follow the redistribution of water in the wide range of pore sizes (see Table 1) during the actual loading of the samples; this was possible uniquely with the ^{1}H NMR.

2. MATERIALS AND METHODS

2.1. Materials, Mixing, and Storage of the Samples.

Cement paste samples were prepared with white Portland cement CEM I 52.5R (Aalborg) at a water-to-cement ratio (w/c) by mass of 0.25, 0.40, and 0.50 by mixing cement with deionized water. For the w/c 0.25 paste only, a polycarboxylate-based liquid superplasticizer (VC 20HE by Sika) was additionally used as partial water replacement in an amount of 0.4% by mass of cement. The plasticizer was necessary to mix the low w/c paste and provide a homogeneous cement paste.

The oxide compositions of the anhydrous cement were (by mass) as follows: SiO_2 24.37%, Al_2O_3 1.97%, Fe_2O_3 0.32%, CaO 68.48% (free CaO 1.35%), MgO 0.70%, K_2O 0.09%, Na_2O 0.16%, SO_3 2.07%. The phase composition of the

DOI: 10.1021/acs.jpcc.9b02436
J. Phys. Chem. C 2019, 123, 16153−16163

cement was as follows (by mass, quantitative X-ray diffractometry): C_3S 71%, C_2S 21%, C_3A 3.2%, C_4AF 0.20%, CH 0.50, anhydrite/gypsum 2.0%, calcite + dolomite 0.50% (according to cement chemistry notation: C_3S−$3CaO{\cdot}SiO_2$, C_2S−$2CaO{\cdot}SiO_2$, C_3A−$3CaO{\cdot}Al_2O_3$, C_4AF−$4CaO{\cdot}Al_2O_3{\cdot}Fe_2O_3$, CH−$Ca(OH)_2$). The cement had a Blaine fineness of 3940 cm^2/g and a density of 3.13 g/cm^3. Thanks to the low C_4AF and C_3A contents of the cement, the interference of the paramagnetic impurities and of the crystalline hydration products like ettringite, respectively, was minimized.

Cement pastes were mixed in batches of about 300 mL in a 500 mL vacuum mixer at 450 rpm for 2 min. After mixing, the pastes were poured into hermetic plastic containers and stored sealed for 16 ± 1 h. Next, miniature cylindrical samples (diameter 7.5 + 0.01/−0.5 mm, height 10 ± 1 mm, mass about 0.9 g) were cored under water using a hardened steel bore. The cylinders were either placed under lime water or kept in sealed conditions (in hermetic plastic containers) until the age of 28 d at 20.0 ± 0.3 °C. Afterward, the samples were conditioned at different controlled relative humidities (RHs) or in sealed conditions to study the effects of the residual moisture conditions in the sample. To this end, the samples were exposed to drying at different RHs in desiccators filled with N_2 (to avoid carbonation) or kept continuously sealed for about 2 years. The RH in desiccators was controlled in the range of 75−98% by means of saturated salt solutions in a climate-controlled room at 20.0 ± 0.3 °C. The masses of the samples were determined at different stages of the conditioning process. The initial (after underwater curing) and final (directly prior to the NMR measurements) mass measurements yielded a sorption isotherm, with reference to dry state determined on the companion samples stored in a desiccator with silica gel. The materials used, sample preparation, and storage procedure were the same as in our previous NMR study.[9]

2.2. Applying Pressure on the Samples. A custom-built pressure cell was used for applying the hydrostatic pressure on cement paste samples during the NMR measurements. The details of the pressure cell are briefly summarized in the Supporting Information, Section S.1. After positioning a cement paste specimen inside the cell and filling the cell with the hydraulic fluid (Krytox GPL 103 fluorinated oil), the cell was placed in the NMR magnet.

At this point, an initial pressure of about 1 MPa was applied to ensure proper filling of the cell with the oil. Next, the NMR coil was tuned with a tuning circuit. After collecting at least two or three NMR measurement datasets, each taking about 17 min, the pressure was applied in a single fast step (shorter than 1 min) with a manual pump (Enerpac). The maximum pressure applied was 150 MPa. Considering that the hydrostatic pressure was applied, this stress level cannot induce failure of the cement paste.[46,47] After applying the pressure, the NMR coil was again tuned (it was found that pressurizing the oil led to a small increase of the NMR coil frequency). Next, the measurements on loaded samples were carried out. The pressure was held nominally constant from about 1 h to about 16 h, depending on the case. Finally, the samples were unloaded back to about 1 MPa. The loading/unloading cycle was in some cases repeated.

The temperature inside the pressure cell, governed by the temperature inside the bore of the magnet, was in the range of 14−16 °C (as measured immediately after removing the cell from the bore of the magnet after having performed a series of measurements).

2.3. NMR Measurements. The ^1H NMR measurements were carried out at 60 MHz using a setup operated at the Department of Physics at the University of Surrey and composed of a superconducting magnet (Magnex), an MRI shim set (Otsuka Electronics) with three gradient amplifiers (Techron), a spectrometer (Kea2 by Magritek), and a pulse amplifier (American Microwave Technology). The magnet has a horizontal bore (diameter 100 mm) accessible from two ends, a feature necessary for accommodating the pressure cell (with the capillary tube connected to the pump at one end and the connection to the electronic control unit at the other end).

The NMR coil placed inside the pressure cell (see the Supporting Information, Figure S1) was made of 4.5 turns of a ø 1.5 mm copper wire. The coil had an internal diameter of 11 mm and a height of 12 mm.

During the measurements, shim coils in three directions were used to compensate for the magnetic field inhomogeneity. The shim current was optimized using a dummy sample made of rubber.

The NMR coil frequency was tuned and matched (the depth of the NMR 'Q' tuning dip and its position were adjusted, respectively) by means of the capacitors and an inductive coil built into the tuning circuit.

The 'mobile' water present in the samples was measured using the Carr−Purcell−Meiboom−Gill (CPMG) pulse sequence. Depending on the sample measured, 192 or 256 linearly spaced echoes from 0.067 to 13 or 18 ms, respectively, were recorded. The $\pi/2$ pulse length was typically equal to 5−6 μs. With a repetition time of 1 s and 1024 averages recorded, one CPMG measurement took about 17 min. The signal-to-noise ratio of the measurements was typically above 2000. More details on the CPMG measurements as applied here can be found in the literature.[35,48]

In addition to measurements on the cell containing a cement paste sample, also measurements with a cell without a sample (but filled with oil) subject to different pressures were run. The small residual signal from the pressurized cell (at 1 or 150 MPa) filled with oil ('empty cell') was subtracted from the signals of the sample at the equivalent pressure.

The masses of the samples were determined before and after the experiments. No change of mass was found for the saturated sample, showing negligible replacement of water with the denser and more viscous oil (density of about 1.9 g/cm^3, dynamic viscosity of about 150 MPa s). For other samples, slight increments of the masses (typically below 5% by mass of the residual water content) were found, likely due to the penetration of the oil into the partially emptied pores. Due to the negligible NMR signal of the oil and the fact that the oil did not mix with the water (as shown by the saturated sample), it can be assumed that the presence of the oil in the pores did not affect the measurements other than by the effect of the hydrostatic pressure.

2.4. Data Deconvolution. The deconvolution of the total CPMG signal decay into different components due to water confined in different pore populations, with their characteristic T_2-values and amplitudes (fractions of the total signal), has proven to be one of the major issues met by ^1H NMR. The deconvolution of the noisy decay data is, in principle, an ill-posed inversion problem, i.e., its solution is not unique.[48,49] Among different methods for the CPMG data deconvolution, inverse Laplace transform (ILT) or methods based on fitting

DOI: 10.1021/acs.jpcc.9b02436
J. Phys. Chem. C 2019, 123, 16153−16163

the sum of single exponential decay components, i.e., multiexponential fitting (with different optimization criteria), are commonly used.[48−50]

Considering that relatively small signal changes needed to be followed, a deconvolution algorithm was required that would provide low variance in the inverted solution between the consecutive scans. Two different ILT algorithms were initially tested,[51,52] and their solutions, i.e., the obtained fractions of different water populations, were significantly different from each other. Moreover, artificial peaks at very low T_2 were often found, see Muller et al.,[48] which seriously limited the number of meaningful results.

On the other hand, a simple multiexponential fitting inversion method (see also the previous studies[9,42]) could provide very stable solutions between the consecutive scans.

In this approach, the total signal decay $S(t)$ as a function of experiment time t (here with linear spacing) is approximated as the sum of the k exponential decay components (each characterized by an amplitude S_k and a relaxation time $T_{2,k}$) that are characteristic of single water populations

$$S(t) \approx \sum_{1}^{k} S_k \exp\left(-\frac{t}{T_{2,k}}\right) \quad (1)$$

The solution is found by minimizing the squared error of fit. In the least-squares optimization, the number of components and their characteristic T_2-relaxation times were constrained for each sample, and their amplitudes (assumed to be the only changing quantity between the consecutive scans) were fitted, similarly as in the previous studies.[9,42] The ILT analysis of the multiple datasets was used to provide the best estimates of the constraints. This yielded a number of peaks $k = 4$ (a small, fifth peak found in some cases was attributed to noise and neglected), in agreement with the previous studies,[9,10,34] and the peaks were thus considered to correspond to the C−S−H interlayer water, gel water, interhydrate water, and capillary water. The characteristic T_2-times to be constrained were averaged between the ILT times obtained from two pressures (1 and 150 MPa). The assumption of the constant T_2 at different pressures is based on the fact that the relaxation rates in porous materials are governed primarily by the interactions of the paramagnetic solid surfaces (pore walls) and the proton in the pore fluid.[53] These interactions are hardly affected by the pressure. Even if the pressure leads to some refinement of the pores (and hence could affect relaxation according to the surface relaxation mechanism), such slight change cannot be resolved considering the measurement and deconvolution uncertainty.

In fact, no significant trend due to pressurization that could indicate a systematic change in T_2 (and hence the change of pore sizes) could be found except for the longest T_2-component (assigned to capillary water), where lower T_2-values were found at a higher pressure. However, the averaged T_2-values still allowed obtaining a good quality of fit.

3. RESULTS

3.1. First Loading Cycle and Reversibility. Clear differences in water populations under pressure were observed for samples preconditioned at 95% RH. These samples are analyzed in this section, while the effect of internal RH is analyzed in Section 3.2.

In Figure 1, the results of pressuring a sample from 1 to 150 MPa are presented. Here and throughout the paper, the

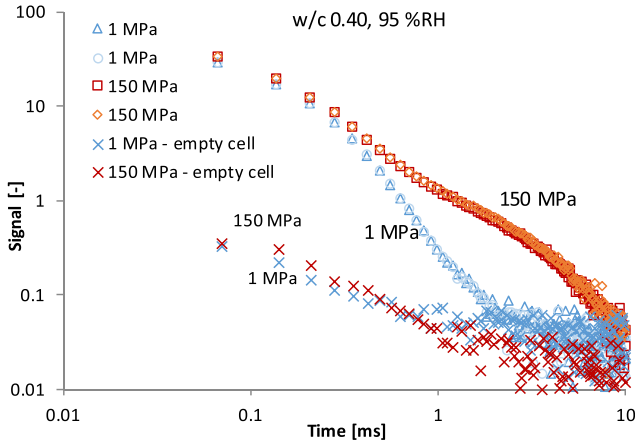

Figure 1. CPMG decay of the w/c 0.40 cement paste sample preconditioned at 95% RH and subject to pressure change from 1 MPa (blue markers) to 150 MPa (red markers). Consecutive (duplicate) measurements at each pressure are shown. The signals of the cell without the sample at two different pressures are also presented.

CPMG decay is presented after subtraction of the signal of the 'empty' (only oil-filled) cavity and phasing. The results of two consecutive measurements at each of the pressures (1 and 150 MPa) are shown (with a time interval of about 17 min between the scans) to indicate the very good repeatability of consecutive measurements (note that the signals at a given pressure, i.e., blue markers at 1 MPa or red markers at 150 MPa, practically overlap in Figure 1).

The data of the cell without the sample ('empty cell') is also presented in Figure 1, showing a very low background signal compared to that of the sample (note the logarithmic scale) that was hardly affected by the application of pressure; the pressure cell itself and the hydraulic fluid can be thus considered to be almost transparent to NMR and not sensitive to pressure.

The application of pressure led to a slight (about 10%) increase in the overall signal amplitude of the sample. This is attributed to the changed tuning of the coil, which varies the Q-factor amplification of the signal. It does not, however, affect the resolved change (redistribution) of the signal.

A clear effect of pressure application can be seen regarding the shape of the decay curve; in particular, for times longer than about 0.5 ms, the signal becomes higher. This already suggests that the redistribution of water from smaller to larger pores takes place due to applied pressure. The signal changes can be approximately assessed if one considers the following characteristic times that mark different pore size populations: times longer than about 0.5 ms correspond to the interhydrate and capillary pores, while times longer than 2 ms correspond to large capillaries only.[6] In this case, it can be seen that the application of pressure causes an increase of the signal fraction of the interhydrate and capillary pores from about 0.07 to 0.10 and of the signal fraction of the capillaries from almost zero to about 0.016 (with the total CPMG signal equal to 1).

Further quantification is made after deconvolution of the total signal with constrained multiexponential fitting (see Section 2.4). As already discussed, this is done with four values of the T_2-times characteristic for different water populations and fixed constant between different pressures within a sample—the changes of amplitudes of different populations are then resolved as an effect of pressure.

DOI: 10.1021/acs.jpcc.9b02436
J. Phys. Chem. C 2019, 123, 16153−16163

In Figure 2a, an example of the multiexponential fit is presented. In Figure 2b, signals for different water populations

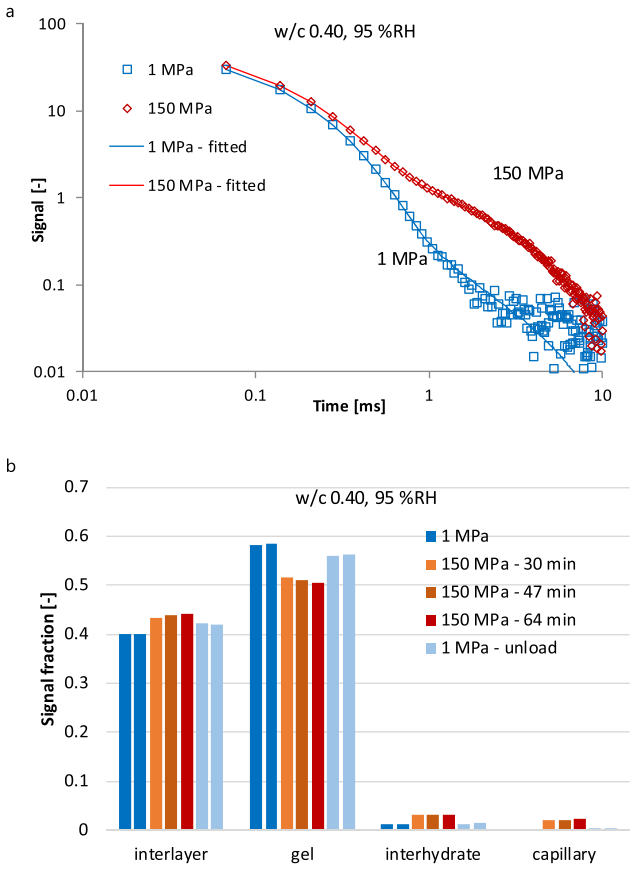

Figure 2. (a) CPMG decay of the w/c 0.40 cement paste sample preconditioned at 95% RH (the same data as in Figure 1) (markers) and the fitted curves obtained with constrained multiexponential fitting (with four fixed T_2-components), and (b) results of data deconvolution with multiexponential fitting. Each bar corresponds to a single CPMG measurement (each measurement lasted about 17 min). Blue bars correspond to 1 MPa and orange-red bars to 150 MPa. Times in the data for 150 MPa denote the time from pressure application to the end of each CPMG measurement.

and their changes due to applied pressure are presented (blue bars correspond to 1 MPa and red bars to 150 MPa). Each bar corresponds to a single measurement within a series. As seen in Figure 2b, the application of pressure causes a decrease in the gel water signal and an increase in signals of other water populations. Part of the gel water is redistributed to larger pores—interhydrate spaces and large capillary pores. In particular, the capillary water, absent in the unloaded sample at this RH (the capillary pores desaturate at high RH[9,10]), appears when pressure is applied. The signal fraction (with all mobile water equal to 1) of the water in large pores (interhydrate + capillary water) increases directly after loading from about 0.015 to about 0.053, i.e., more than three times. Another effect related to the decrease of the gel water signal fraction is the increase of the signal fraction corresponding to the shortest resolved T_2. Although this shortest T_2-component is attributed to the water under strongest interaction with the solids, i.e., the C−S−H interlayer water, it should be anticipated here that the increase of this signal fraction upon loading does not necessarily mean that it is due to the amount of the interlayer water that changed. Its major part is likely due to the refinement of some part of the gel pores to a size whereby they are resolved as the interlayer spaces. This is consistent through all of the results presented thereafter and will be discussed in detail in Section 4.

When the sample is unloaded, the changes in large pores are practically fully reversible. This is not the case for the interlayer signal fraction, where only part of the change is recovered.

As long as the shape of the signal decay curve between consecutive measurements at 1 MPa is rather constant (see blue bars in Figure 2b), the temporal evolution of the signal can be seen after applying pressure. This is studied in detail in Section 3.4.

The repeatability of the experiment has been also assessed by testing thee samples of w/c 0.40 produced in different mixings and all preconditioned at 95% RH. The tests were run at different times (across a couple of months), i.e., with different settings of the NMR magnet. The changes of the signal after applying pressure presented in Figure 3 appear to

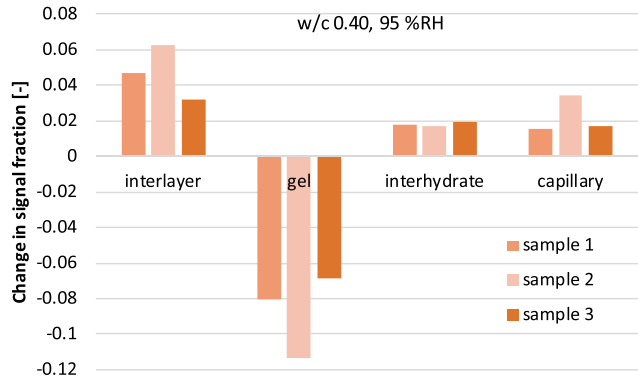

Figure 3. Changes in signal fractions (with total CPMG signal equal to 1) of different water populations at increasing pressure from 1 to 150 MPa obtained with constrained multiexponential fitting for triplicate samples of the w/c 0.40 cement paste preconditioned at 95% RH.

be fairly repeatable across different samples, indicating the good repeatability of the experiment (in addition to good repeatability for a single sample between consecutive measurements, as already shown in Figure 1).

3.2. Second Loading Cycle. The second loading cycle was applied to the same sample, as presented in Section 3.1 (w/c 0.40, preconditioned at 95% RH). After the first unloading back to 1 MPa, two CPMG measurements were run (light blue bars presented in Figure 2b) and the sample was again loaded to 150 MPa. After taking three further CPMG measurements, the pressure was reduced to 100 MPa and next again to 1 MPa. The signal changes during the second loading cycle were similar to those during the first loading cycle, as shown by the comparison in Figure 4. The results of the second cycle as revealed by the multiexponential fitting are presented in the Supporting Information, Figure S2.

It can be seen that the redistribution of water populations due to loading/unloading pressure is repeatable during subsequent cycles. However, unloading to only 100 MPa did not lead to any visible effect compared to that of 150 MPa (see Figure S2 in the Supporting Information). It was also found on a number of samples at different RHs (results not presented here) that loading a sample from 1 to 100 MPa or further to 120 MPa did not lead to any significant change in the signal

DOI: 10.1021/acs.jpcc.9b02436
J. Phys. Chem. C 2019, 123, 16153−16163

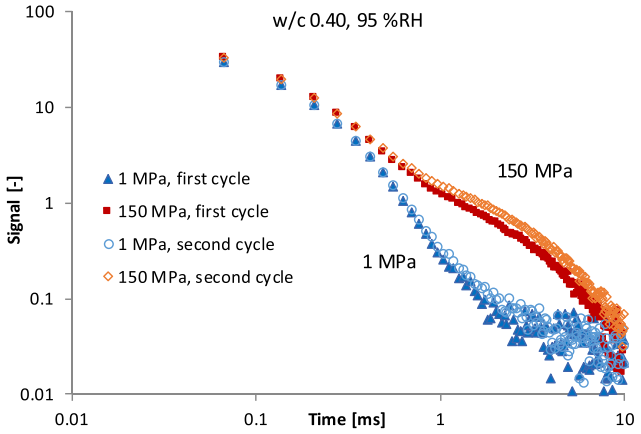

Figure 4. CPMG decay of the w/c 0.40 cement paste preconditioned at 95% RH during the first and the second loading cycles.

(while the change occurred after subsequently increasing the pressure to 150 MPa). The possible reasons are further discussed in Section 4.

3.3. Effect of Residual RH on Redistribution Under Pressure. Samples of the w/c 0.40 cement paste at different RHs were tested: 75, 85, 95, and 98%, and stored under water (nominally saturated). In Figure 5, the effect of pressure on the

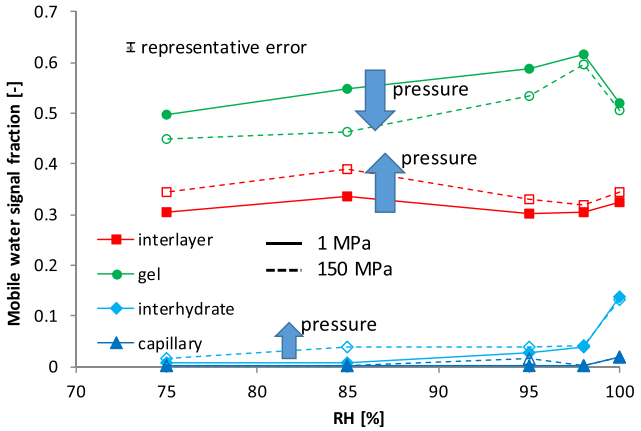

Figure 5. Signal fractions of different water populations in the w/c 0.40 cement paste measured at 1 MPa (continuous lines) and in the first CPMG measurement after changing the pressure to 150 MPa (dashed lines) as a function of internal RH prior to the experiment. The total signals of different samples were normalized based on gravimetric sorption isotherm measurements. 100 %RH corresponds to samples stored under water.

redistribution of water populations is presented as a function of the internal RH in the samples (assumed equal to the RH at which the samples were conditioned prior to the experiments). The continuous lines show the water populations as revealed by multiexponential fitting on the CPMG scans collected at 1 MPa (in the last scan before increasing the pressure), and the dashed lines were obtained from the CPMG scans directly after applying the 150 MPa pressure (i.e., the first CPMG measurement starts about 15 min from changing the pressure). The change at 95% RH is that presented already in Section 3.1, Figure 2b. The total signal amplitudes at each RH are normalized based on the desorption isotherm obtained from mass measurements on duplicate samples conditioned in the desiccators prior to the NMR measurements. The error bar in Figure 5 represents the standard deviation resulting from the joint average variances of the NMR measurements and the gravimetric measurements. The former was obtained from the variance of the consecutive NMR measurements (after deconvolution) of single samples at 1 MPa pressure and the latter from the variance in mass change measurements of duplicate samples.

As can be seen in Figure 5, the redistribution of water signal under pressure is similar in the samples in the range of 75–95% RH. At higher RH (98% and in saturated samples), the redistribution was lower and limited only to the change of signal from gel to interlayer water.

3.4. Temporal Evolution of Signal After Loading. Despite its relatively low magnitude, a clear temporal evolution of the signal could be observed in most of the samples. In Figure 6, it is presented for the samples conditioned at 95, 85, and 75% RHs. The corresponding deconvolution of the signal with multiexponential fitting is presented in the Supporting Information, Figure S3a–c, respectively. According to the deconvolution results, the temporal evolution of the signal corresponded to both the redistribution between the gel water and water in larger pores (interhydrate + capillary) and between the gel water and water in smaller pores (resolved as the interlayer water). The analysis of the changing signal for the exemplary case of the sample conditioned at 85% RH, Figure 7, shows that the water changes can be well fitted with linear trends in the short time range observed here. For other samples conditioned at 75 and 95% RHs, the rates of signal change were similar to those presented in Figure 7 (approximately linear in time).

The change under pressure and the temporal evolution of the signal were also observed for a w/c 0.25 sample cured in sealed conditions (i.e., undergoing self-desiccation), Figure 8. The corresponding deconvolution of the signal is presented in the Supporting Information, Figure S3d. In this sample, a residually low amount of water in larger pores with a signal fraction of around 0.012 increased to 0.022 after loading (this value was stable over 17 h). Even though a clear temporal evolution could be observed in the CPMG decays during the first hour after loading, it corresponds to very small changes in the deconvoluted data. After about 17 h under load, redistribution from gel to interlayer signal could be observed. The recovery upon unloading regarded only the largest pores.

It should be noted that the relaxation behavior in the w/c 0.25 paste may have been affected by the presence of the superplasticizer. The plasticizer adsorbed on the solid surfaces (pore walls) hinders the access of the pore fluid to the surfaces (hydrophobic effect).[54,55] This should lead to lower relaxation rates of protons in the pore fluid.[56,57] Further, a contribution of the proton in the superplasticizer is possible and should be, however, less significant considering the small concentration of the organic superplasticizer in the mixing water (1.6% by mass). At the same time, such systematic effects should be uniform at different pressures. Hence, the net effect of pressurizing on water redistribution should be still valid and independent from the altered surface relaxivity.

4. DISCUSSION

4.1. Summary of the Results. The presented results show that the redistribution of water (microdiffusion) between different classes of pores within the microstructure of hardened cement paste takes place under mechanical (here hydrostatic) loading.

DOI: 10.1021/acs.jpcc.9b02436
J. Phys. Chem. C 2019, 123, 16153–16163

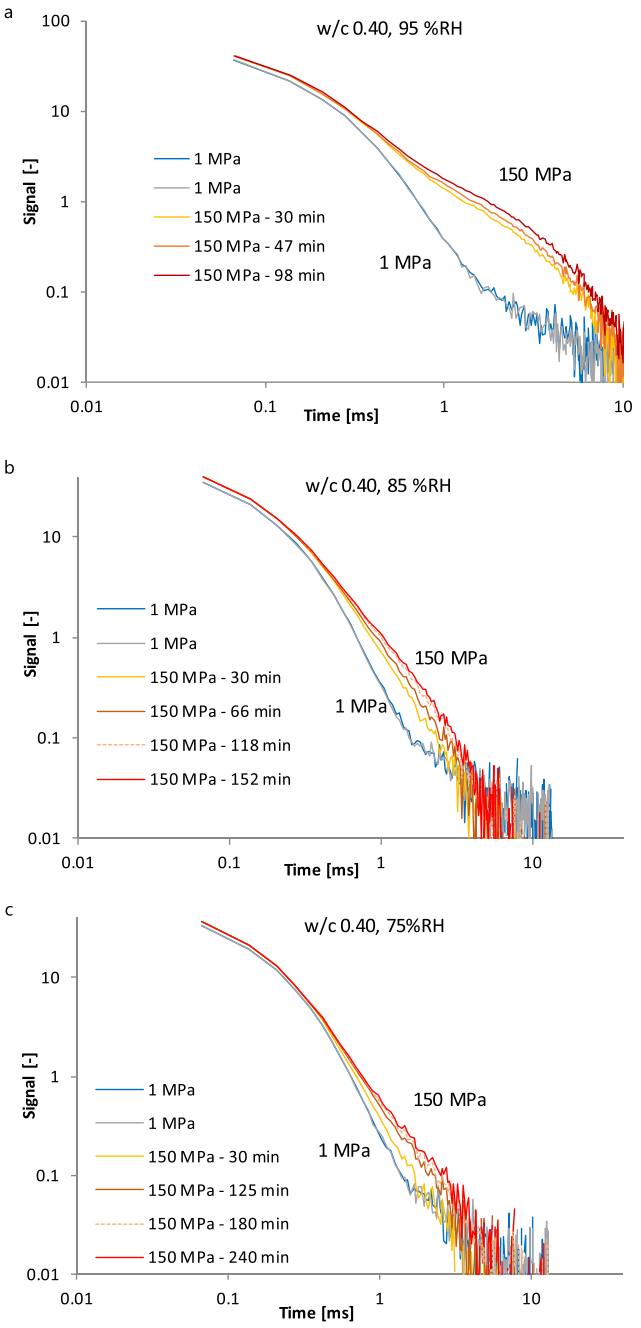

Figure 6. CPMG decays: effect of applying pressure (150 MPa) on the w/c 0.40 cement paste preconditioned at (a) 95% RH, (b) 85% RH, and (c) 75% RH. The temporal evolution of the signal after loading can be seen. Each curve corresponds to a single consecutive CPMG measurement. Blue curves correspond to 1 MPa and orange-red curves to 150 MPa. Times in the data for 150 MPa denote the times from pressure application to the end of each CPMG measurement. The deconvolution of the signal is presented in the Supporting Information, Figure S3a–c.

Upon applying hydrostatic pressure, the shapes of the CPMG decay curves change, suggesting the movement of water to larger pores. After a more detailed analysis of the CPMG decays with constrained multiexponential fitting, it can be seen that pressurizing the unsaturated (i.e., preconditioned at below 98% RH) samples leads to a clear reduction of the gel water signal. This signal becomes redistributed into the following signals: (1) corresponding to water in the

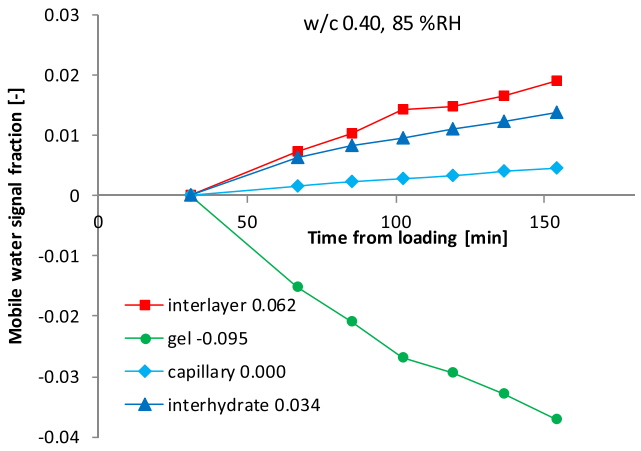

Figure 7. Change of the signal fractions in time of different water populations in a w/c 0.40 sample preconditioned at 85% RH occurring after the first CPMG measurement at 150 MPa pressure, as revealed by the multiexponential fitting (the deconvoluted results are presented in the Supporting Information, Figure S3b). Time for each data point is the time between the application of pressure and the end of each measurement. Note that the signal changes found in the first CPMG measurement after increasing the pressure (i.e., between zero and the first point on the curves at about 30 min) were: gel −0.095, interlayer +0.062, interhydrate +0.034, capillary 0.000.

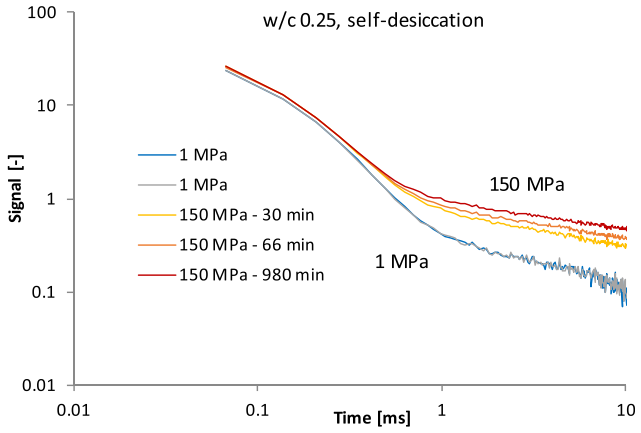

Figure 8. CPMG decays of the w/c 0.25 cement paste preconditioned in sealed conditions. Each curve corresponds to a single consecutive CPMG measurement. Blue curves correspond to 1 MPa and orange-red bars to 150 MPa. Times in the data for 150 MPa denote the time from pressure application to the end of each CPMG measurement.

interhydrate and capillary pores, i.e., larger pores, and (2) corresponding to water with relaxation time shorter than that for the gel pores, i.e., smaller pores. Process (1) can be readily interpreted as due to migration of water from smaller (gel) to larger pores. This part of the signal change is almost fully reversible. Process (2) is resolved in the signal deconvolution as an increase in the interlayer C−S−H water signal and is only partially reversible after first unloading. In samples close to saturation (preconditioned at 98% RH or under water), redistribution of the signal under pressure is much lower and regards only the increase of the interlayer water signal at the expense of the gel signal.

Even though the amount of water redistributed upon loading is in absolute terms rather small (a couple of percentage of all water), it is not negligible, especially considering its relative magnitude compared to the residual amount of water in the

DOI: 10.1021/acs.jpcc.9b02436
J. Phys. Chem. C 2019, 123, 16153−16163

largest pores to which the water migrates. In fact, in the capillary pores that are emptied of water already at about 95% RH (see the NMR desorption experiments by Muller et al.[10]), water reappears when the sample is compressed. In general, in the range of 75−95% RH, the amount of water in the largest pores (interhydrate + capillary) increased to about 2−3 times upon loading. It should be stressed here that the distinction between the two classes of the largest pores, interhydrate and capillary, is subject to high uncertainty.

The process of redistribution was time-lapsed; the quantification of the rates is, however, hardly possible due to the relatively short times of the experiments on one hand and the coarse temporal resolution of the NMR measurements on the other hand, not allowing to resolve the initial (supposedly fast) redistribution kinetics. All analyzed samples preconditioned at different RHs (75−100%) had similar rates of signal change.

4.2. Proposed Mechanism. Based on the results presented above and on previous works,[58,59] we postulate the following mechanism to explain the water redistribution upon hydrostatic loading. In a saturated sample, no redistribution to large pores is possible as these pores are already filled with water and no further transport is possible under hydrostatic loading. Additionally, the small amounts of water that might migrate between different sizes of the largest pores (should part of them be empty prior to loading) can probably not be detected with the present method. This effect likely contributes also to the relatively small redistribution seen at 98% RH.

On the other hand, when the sample is unsaturated (below 98% RH), water in the saturated part of the gel pores can diffuse when stressed to available free spaces, i.e., larger pores. These are previously unsaturated capillary voids (at high RH) or interhydrate spaces (at intermediate RH). This generally validates the hypothesis of microdiffusion in the form put forward previously.[4,24]

The fact that the signal resolved as the interlayer water also increases at the expense of the gel water cannot be readily explained with the creation of new C−S−H with its interlayer water in a hydration process. First, such a process could only explain the irreversible part of the signal change (bear in mind that about half of the interlayer signal increase is reversible upon unloading). Although it is, in principle, possible that the hydrostatic pressure could enhance the dissolution of the remaining anhydrous cement and hence provoke some further hydration while under load,[60] we stress that the irreversible increase of the signal fraction occurred also in samples that were relatively short under load, about 1 or 3 h. Hence, considering a relatively high residual hydration degree, one can expect very little increase of hydration in such short time.

Instead, we suggest that the increase of the interlayer signal fraction is not due to the actual increase in the interlayer water, but due to the refinement of small gel pores that are similar in size and hence in the corresponding T_2 (within the resolution limit of the deconvolution method) to the interlayer spaces. Note that exponential fitting allows only a discrete number of T_2-components to be assigned rather than a continuous distribution. The partially irreversible signal redistribution can be explained by a possible permanent rearrangement of the gel porosity.

According to recent observations,[34] gel pores are spaces formed between the stacks of C−S−H sheets. We postulate that when the gel water migrates under compression to capillary pores, the opposite walls of the gel pores move toward each other, possibly creating finer pores close in size to the C−S−H interlayers. In an extreme situation, opposite stacks of C−S−H sheets separated by a deformable gel space (with water kept inside) come together as the water is expelled to form a thicker stack with entrapped interlayer-like water. In any case, the gel pores might be compressed and water confined in them may reach a relaxation time similar to that of the interlayer or adsorbed water, thus increasing the signal of the latter. The reason for the refinement of the gel pores may be not only due to the water migrating out but at the same time also due to the intrinsically viscoelastic behavior of the solid gel. It should be noted that the rates of the increase of the signal of the interlayer C−S−H water are similar to those of the large (capillary + interhydrate) pores; thus, it appears that the two effects, i.e., water migrating out of gel porosity and its confinement, are linked through one diffusion process.

We note that we see a small effect upon loading at 150 MPa but did not see an effect at loading from 1 to 100 or 120 MPa. One could attribute this to the small size of the change and sensitivity of the measurement. However, it is curious that Maruyama et al.[61] have recently reported that cavitation in cement paste during desorption occurs at a pressure of −140 MPa. This observation aided with the Laplace equation led to the conclusion that the larger gel pores are constricted by neck entrances of sizes below about 2 nm (i.e., very small gel pores). The changes seen here somehow "switched on" somewhere between 120 and 150 MPa. It may be that these results are connected if we assume the following hypothetical mechanism. We see a clear change in water populations only once the pressure of about 120−150 MPa is exerted because only then the pressure in the (supposedly) gel water becomes high enough for the water to be pressed out through small (below about 2 nm) neck entrances and emerge as different water population (interlayer or capillary water).

4.3. Water Migration and Changes of RH. The process of fast migration of water primarily to large pores under loading is in line with the macroscopic measurements of RH in mortars under uniaxial compression.[58,59] It was found that the compression of the w/c 0.30 mortar samples caused an immediate increase of RH (about 2% at 30 MPa) and that the change in RH was proportional to the applied stress. The process was reversible upon unloading. The increase of RH was explained (based on the hypothesis proposed originally by Powers[15,17]) by water moving to larger pores from hindered adsorption areas, thus decreasing the curvature of the menisci. We now complement this hypothesis by stating that the observed RH changes under pressure are caused by water moving primarily from gel pores to interhydrate spaces (according to the pore size classification by ^{1}H NMR).

In our previous study,[9] we focused on the influence of temperature on water redistribution. It was found that heating causes an immediate redistribution of the NMR signal from the interlayer to primarily gel pores and to a lesser extent to the interhydrate and capillary pores. The movement of water toward larger pores could explain the increase of RH upon heating (similarly as here the increase under compression is explained by migration). The larger fraction of water undergoing redistribution due to temperature compared to that observed here during mechanical loading is in line with the fact that temperature changes cause larger changes of the RH (about 0.5%/°C[62]) than the mechanical loading.

The difference of the source pores (interlayer upon heating and larger gel pores upon compression) during migration can

DOI: 10.1021/acs.jpcc.9b02436
J. Phys. Chem. C 2019, 123, 16153−16163

be due to different driving forces. The water confined in the interlayer spaces has lower entropy compared to the gel and capillary water that can be both treated as bulk water and should possibly have similar entropy.[30,31,63] When the temperature increases, a difference of chemical potential is therefore established between the interlayer water and gel water that exist in its immediate vicinity, which causes an almost instantaneous migration from the interlayer to gel spaces.[9] Additionally, opening up of interlayer spaces to form larger (gel) voids could take place as backbone sheets of C−S−H deform upon heating and water confined between them expands due to thermal deformation (similarly to the "unzipping" of C−S−H observed upon rewetting[42]).[9]

On the other hand, when the microstructure is compressed (here hydrostatically), the deformation will locally take place primarily at the expense of pores filled with the least dense species, i.e., first empty pores and pores filled with bulk water. The load-bearing water confined in the C−S−H interlayers should possibly have higher density[64] and strongly interact with the solids. Consequently, the C−S−H interlayer spaces should have lower compressibility, leading also to lower mobility of the confined water under mechanical loading. The low deformability of the C−S−H interlayer spaces was reported by Geng et al.,[65] who at a hydrostatic pressure of 1 GPa (i.e., 1 order of magnitude higher than applied here) observed strains in C−S−H lattice equal to a fraction of percent only.

4.4. Water Migration and Creep. An important question is how the observed migration of water relates to short-term creep. As discussed in the introduction, time-lapsed microdiffusion of load-bearing water was often proposed to explain the short-term, reversible creep component.[22,24,26−29]

We postulate that the fast migration of water (occurring likely within seconds but measured with NMR only at a temporal resolution of about 15−30 min) is likely responsible for the very short-term creep occurring already from the time instant of loading. The fast redistribution and corresponding change of RH were proposed to be responsible for the static Young's modulus being lower than the dynamic modulus.[58]

As for the time-lapsed diffusion of water responsible for short-term reversible creep, we can cautiously confirm this hypothesis based on our data. A possible alternative mechanism needs to be, however, mentioned. In this mechanism, the migration of water is merely the effect of the intrinsically viscoelastic deformation of the solid gel that contracts and refines (leading to the resolving part of the gel water now as the interlayer water) and forcing part of the water to larger voids, but without any contribution of such water to bearing stress and hence to deformation.

It should also be stressed that, despite confirming the time-lapsed migration of water, drawing detailed conclusions and quantification of the microdiffusion rate is currently impossible due to the very small magnitude of the NMR signal change and the uncertainties related to data deconvolution.

The applied hydrostatic loading used in our test was different from the uniaxial compressive loading used in most creep tests. The higher strength in triaxial compression[46,47] (here hydrostatic) allowed us to use pressures of up to 150 MPa without failure of the samples (note that at a pressure of about 100 MPa, no effect of redistribution could be observed; hence, such high pressure was necessary). A question is how the hydrostatic load corresponds to the uniaxial load in terms of the deformations (and water redistribution) at the microstructural level. The hydrostatic load applied here most likely led to higher volumetric deformation (contraction) than the uniaxial load used commonly in the creep tests. To the best of our knowledge, large volumetric deformations under hydrostatic loading leading to the reduction of porosity (and supposedly to water migration out of the compacted pores) were reported only in a paper by Bernard et al.[21] At the same time, even though deviatoric strains can be expected at the microscopic level even under the hydrostatic load,[21] they would be still higher in the case of the uniaxial load. The initial fast reduction of porosity (until about 2 h from loading) measured by Bernard et al. was followed by slower reduction that ceased at about 23 d.[21] Our observations of water migration (both the confirmation of the process and possibly also its temporal evolution) are therefore consistent with the available hydrostatic creep data.[21] Considering that volumetric creep (contraction) was found to be smaller under deviatoric loading,[21] the magnitude of water migration may be smaller under uniaxial compression than reported here for the hydrostatic compression.

5. CONCLUSIONS

We used ^{1}H NMR to study the redistribution of water in cement pastes under a hydrostatic loading of up to 150 MPa. During compression of unsaturated samples (w/c 0.25 after sealed curing or w/c 0.40 after storage at 75−95% RH), water redistribution from gel pores to larger (interhydrate and capillary) pores takes place (i.e., from smaller to larger mesopores and macropores, respectively, according to the IUPAC classification[8]). Due to this redistribution, the NMR signal fraction due to the largest pores increases even 2−3 times. This process is almost fully reversible upon unloading. At the same time, an increase of the signal attributed to the shortest relaxation time, i.e., the signal interpreted as the interlayer water, was observed with a magnitude similar to that of the increase in the largest pores. We propose that this is primarily due to rearrangement of the gel upon compression and refinement of the part (around 5−10%) of the gel porosity as water stored in it is expelled during compression. As a consequence, smaller gel pores are created that are close in size to the interlayer spaces (and hence, water in them experiences similar relaxation time). Such a process is partially reversible, while the irreversible part could be due to a permanent rearrangement of porosity. Although it is virtually possible that the irreversible part of the increase in the interlayer water signal fraction is due to the advanced hydration under pressure, we find such a process unlikely considering a relatively short time under pressure. A verification of the possible increase of hydration degree would require solid-echo measurements that could resolve solid-like hydrogen (with a relaxation time T_2 of about 10−20 μs) present in the crystalline hydration products.[66] Such measurements could not be carried out in our study due to a too long spectrometer dead time in the NMR setup used.

In samples close to saturation (preconditioned at 98% RH and under water), the changes in the signal were considerably lower and regarded only small redistribution between the gel and interlayer signals, i.e., rearrangement/refinement of gel porosity likely took place. This is likely because larger pores were full of water prior to applying pressure and hence could not accommodate any more water from gel pores under hydrostatic pressure.

DOI: 10.1021/acs.jpcc.9b02436
J. Phys. Chem. C 2019, 123, 16153−16163

Most of the water is displaced, and most of the refinement of gel porosity takes place immediately after loading (before the first measurement is concluded after about 30 min), followed by time-lapsed redistribution and refinement that could be observed during several hours under load. Precise quantification of the time-lapsed migration is not possible due to the small amounts of water involved in the process and the uncertainties of the data inversion methods. Nevertheless, the process could be qualitatively confirmed.

These results are in line with the previous observations of porosity reduction over time in hydrostatically compressed pastes or mortars. Our results allow us to confirm the hypothesis that quasi-immediate water redistribution to larger pores is responsible for RH increase upon compression. Further, our results appear to support the hypothesis of water migration (microdiffusion) as responsible for short-term creep.

■ ASSOCIATED CONTENT

Supporting Information

The Supporting Information is available free of charge on the ACS Publications website at DOI: 10.1021/acs.jpcc.9b02436.

Pressure cell used for measuring cement paste samples under varying hydrostatic pressure in NMR magnet (Figure S1); and results of data deconvolution with multiexponential fitting showing the effect of applying pressure (Figure S2 and Figure S3) (PDF)

■ AUTHOR INFORMATION

Corresponding Author

*E-mail: mateusz.wyrzykowski@empa.ch. Tel: +41587654541.

ORCID

Mateusz Wyrzykowski: 0000-0003-1995-6638

Notes

The authors declare no competing financial interest.

■ ACKNOWLEDGMENTS

The study presented here was funded by the Swiss National Science Foundation (SNSF) within the framework of the Ambizione grant of Mateusz Wyrzykowski (project 161414, "Role of water redistribution in creep of concrete"). The authors would like to thank Mr. Erich Heiniger (Empa) for his help in the construction of the pressure cell and Mr. Janis Justs (Empa) for his help in the testing of the cell.

■ REFERENCES

(1) Hansen, T. Physical Structure of Hardened Cement Paste. A Classical Approach. *Mater. Struct.* **1986**, *19*, 423−436.

(2) Wittmann, F. H. Interaction of Hardened Cement Paste and Water. *J. Am. Ceram. Soc.* **1973**, *56*, 409−415.

(3) Powers, T. C.; Brownyard, T. L. *Studies of the Physical Properties of Hardened Portland Cement Paste*, ACI Journal Proceedings. ACI, 1946.

(4) Acker, P. Swelling, Shrinkage and Creep: A Mechanical Approach to Cement Hydration. *Mater. Struct.* **2004**, *37*, 237−243.

(5) Jennings, H. M. Colloid Model of C−S−H and Implications to the Problem of Creep and Shrinkage. *Mater. Struct.* **2004**, *37*, 59−70.

(6) McDonald, P. J.; Rodin, V.; Valori, A. Characterisation of Intra- and Inter-C−S−H Gel Pore Water in White Cement Based on an Analysis of NMR Signal Amplitudes as a Function of Water Content. *Cem. Concr. Res.* **2010**, *40*, 1656−1663.

(7) Lura, P.; Jensen, O. M.; van Breugel, K. Autogenous Shrinkage in High-Performance Cement Paste: An Evaluation of Basic Mechanisms. *Cem. Concr. Res.* **2003**, *33*, 223−232.

(8) Burwell, R. L. In Section 1 - Definitions and Terminology. *Manual of Symbols and Terminology for Physicochemical Quantities and Units−Appendix II*; Burwell, R. L., Ed.; Pergamon, 1976; pp 74−86.

(9) Wyrzykowski, M.; McDonald, P. J.; Scrivener, K. L.; Lura, P. Water Redistribution within the Microstructure of Cementitious Materials Due to Temperature Changes Studied with ^{1}H NMR. *J. Phys. Chem. C* **2017**, *121*, 27950−27962.

(10) Muller, A. C. A.; Scrivener, K. L.; Gajewicz, A. M.; McDonald, P. J. Use of Bench-Top NMR to Measure the Density, Composition and Desorption Isotherm of C−S−H in Cement Paste. *Microporous Mesoporous Mater.* **2013**, *178*, 99−103.

(11) Valori, A.; McDonald, P. J.; Scrivener, K. L. The Morphology of C−S−H: Lessons from ^{1}H Nuclear Magnetic Resonance Relaxometry. *Cem. Concr. Res.* **2013**, *49*, 65−81.

(12) Jennings, H. M. Refinements to Colloid Model of C−S−H in Cement: CM-II. *Cem. Concr. Res.* **2008**, *38*, 275−289.

(13) Korb, J. P. NMR and Nuclear Spin Relaxation of Cement and Concrete Materials. *Curr. Opin. Colloid Interface Sci.* **2009**, *14*, 192−202.

(14) Jennings, H. M.; Kumar, A.; Sant, G. Quantitative Discrimination of the Nano-Pore-Structure of Cement Paste During Drying: New Insights from Water Sorption Isotherms. *Cem. Concr. Res.* **2015**, *76*, 27−36.

(15) Powers, T. C. *Mechanisms of Shrinkage and Reversible Creep of Hardened Cement Paste*, Proceedings of the International Symposium on Structural Concrete, London, 1965; pp 319−344.

(16) Beltzung, F.; Wittmann, F. H. Role of Disjoining Pressure in Cement Based Materials. *Cem. Concr. Res.* **2005**, *35*, 2364−2370.

(17) Powers, T. C. The Thermodynamics of Volume Change and Creep. *Mater. Struct.* **1968**, *1*, 487−507.

(18) Bažant, Z. P. Thermodynamics of Interacting Continua with Surfaces and Creep Analysis of Concrete Structures. *Nucl. Eng. Des.* **1972**, *20*, 477−505.

(19) Bazant, Z. P.; Chern, J. C. Concrete Creep at Variable Humidity: Constitutive Law and Mechanism. *Mater. Struct.* **1985**, *18*, 1−20.

(20) Grasley, Z.; Lange, D. The Viscoelastic Response of Cement Paste to Three-Dimensional Loading. *Mech. Time-Depend. Mater.* **2007**, *11*, 27−46.

(21) Bernard, O.; Ulm, F.-J.; Germaine, J. T. Volume and Deviator Creep of Calcium-Leached Cement-Based Materials. *Cem. Concr. Res.* **2003**, *33*, 1127−1136.

(22) Acker, P.; Ulm, F.-J. Creep and Shrinkage of Concrete: Physical Origins and Practical Measurements. *Nucl. Eng. Des.* **2001**, *203*, 143−158.

(23) Vandamme, M.; Ulm, F.-J. Nanogranular Origin of Concrete Creep. *Proc. Natl. Acad. Sci. U.S.A.* **2009**, *106*, 10552−10557.

(24) Feldman, R. F. Mechanism of Creep of Hydrated Portland Cement Paste. *Cem. Concr. Res.* **1972**, *2*, 521−540.

(25) Bažant, Z.; Hauggaard, A.; Baweja, S.; Ulm, F. Microprestress-Solidification Theory for Concrete Creep. I: Aging and Drying Effects. *J. Eng. Mech.* **1997**, *123*, 1188−1194.

(26) Wittmann, F. H. Creep and Shrinkage Mechanisms. *Creep and Shrinkage in Concrete Structures*, 1982; pp 129−161.

(27) Hilaire, A.; Benboudjema, F.; Darquennes, A.; Berthaud, Y.; Nahas, G. Modeling Basic Creep in Concrete at Early-Age under Compressive and Tensile Loading. *Nucl. Eng. Des.* **2014**, *269*, 222−230.

(28) Pichler, C.; Lackner, R. A Multiscale Creep Model as Basis for Simulation of Early-Age Concrete Behavior. *Comput. Concr.* **2008**, *5*, 295−328.

(29) Sercombe, J.; Hellmich, C.; Ulm, F.-J.; Mang, H. Modeling of Early-Age Creep of Shotcrete. I: Model and Model Parameters. *J. Eng. Mech.* **2000**, *126*, 284−291.

(30) Bažant, Z. P. Delayed Thermal Dilatations of Cement Paste and Concrete Due to Mass Transport. *Nucl. Eng. Des.* **1970**, *14*, 308−318.

(31) Sellevold, E.; Bjøntegaard, Ø. Coefficient of Thermal Expansion of Cement Paste and Concrete: Mechanisms of Moisture Interaction. *Mater. Struct.* **2006**, *39*, 809−815.

DOI: 10.1021/acs.jpcc.9b02436
J. Phys. Chem. C 2019, 123, 16153−16163

(32) Friedemann, K.; Stallmach, F.; Kärger, J. NMR Diffusion and Relaxation Studies During Cement Hydration—a Non-Destructive Approach for Clarification of the Mechanism of Internal Post Curing of Cementitious Materials. *Cem. Concr. Res.* **2006**, *36*, 817−826.
(33) Chary, K. V. R.; Govil, G. Basic Concepts in NMR Spectroscopy. *NMR in Biological Systems: From Molecules to Humans*; Chary, K. V. R.; Govil, G., Eds.; Springer Netherlands: Dordrecht, 2008; pp 1−41.
(34) Muller, A. C. A.; Scrivener, K. L.; Gajewicz, A. M.; McDonald, P. J. Densification of C−S−H Measured by ^{1}H NMR Relaxometry. *J. Phys. Chem. C* **2013**, *117*, 403−412.
(35) Gajewicz, A. Characterisation of Cement Microstructure and Pore − Water Interaction by ^{1}H Nuclear Magnetic Resonance Relaxometry. Ph.D. Thesis, University of Surrey, 2014.
(36) Pirazzoli, I.; Alesiani, M.; Capuani, S.; Maraviglia, B.; Giorgi, R.; Ridi, F.; Baglioni, P. The Influence of Superplasticizers on the First Steps of Tricalcium Silicate Hydration Studied by NMR Techniques. *Magn. Reson. Imaging* **2005**, *23*, 277−284.
(37) Tritt-Goc, J.; Piślewski, N.; Kościelski, S.; Milia, F. The Influence of the Superplasticizer on the Hydration and Freezing Processes in White Cement Studied by ^{1}H Spin-Lattice Relaxation Time and Single Point Imaging. *Cem. Concr. Res.* **2000**, *30*, 931−936.
(38) Faure, P. F.; Rodts, S. Proton NMR Relaxation as a Probe for Setting Cement Pastes. *Magn. Reson. Imaging* **2008**, *26*, 1183−1196.
(39) Fischer, N.; Haerdtl, R.; McDonald, P. J. Observation of the Redistribution of Nanoscale Water Filled Porosity in Cement Based Materials During Wetting. *Cem. Concr. Res.* **2015**, *68*, 148−155.
(40) Hu, Z.; Wyrzykowski, M.; Scrivener, K.; Lura, P. A Novel Method to Predict Internal Relative Humidity in Cementitious Materials by ^{1}H NMR. *Cem. Concr. Res.* **2018**, *104*, 80−93.
(41) Huang, H.; Ye, G.; Pel, L. New Insights into Autogenous Self-Healing in Cement Paste Based on Nuclear Magnetic Resonance (NMR) Tests. *Mater. Struct.* **2016**, *49*, 2509−2524.
(42) Gajewicz, A. M.; Gartner, E.; Kang, K.; McDonald, P. J.; Yermakou, V. A ^{1}H NMR Relaxometry Investigation of Gel-Pore Drying Shrinkage in Cement Pastes. *Cem. Concr. Res.* **2016**, *86*, 12−19.
(43) van der Heijden, G. H. A.; Pel, L.; Adan, O. C. G. Fire Spalling of Concrete, as Studied by NMR. *Cem. Concr. Res.* **2012**, *42*, 265−271.
(44) Muller, A. C. A.; Scrivener, K. L. A Reassessment of Mercury Intrusion Porosimetry by Comparison with ^{1}H NMR Relaxometry. *Cem. Concr. Res.* **2017**, *100*, 350−360.
(45) Bahafid, S. A Multi-Technique Investigation of the Effect of Hydration Temperature on the Microstructure and Mechanical Properties of Cement Paste. Ph.D. Thesis, Paris Est, 2017.
(46) Lu, X.; Hsu, C.-T. T. Behavior of High Strength Concrete with and without Steel Fiber Reinforcement in Triaxial Compression. *Cem. Concr. Res.* **2006**, *36*, 1679−1685.
(47) Imran, I.; Pantazopoulou, S. Experimental Study of Plain Concrete under Triaxial Stress. *ACI Mater. J.* **1996**, *93*, 589−601.
(48) Muller, A. C. A.; Mitchell, J.; McDonald, P. J. Proton Nuclear Magnetic Resonance Relaxometry. In *A Practical Guide to Microstructural Analysis of Cementitious Materials*; Scrivener, K.; Snellings, R.; Lothenbach, B., Eds.; CRC Press, 2015.
(49) Ghosh, S.; Keener, K. M.; Pan, Y. A Simulation Based Method to Assess Inversion Algorithms for Transverse Relaxation Data. *J. Magn. Reson.* **2008**, *191*, 226−230.
(50) Borgia, G. C.; Brown, R. J. S.; Fantazzini, P. Uniform-Penalty Inversion of Multiexponential Decay Data. *J. Magn. Reson.* **1998**, *132*, 65−77.
(51) Provencher, S. W. Contin: A General Purpose Constrained Regularization Program for Inverting Noisy Linear Algebraic and Integral Equations. *Comput. Phys. Commun.* **1982**, *27*, 229−242.
(52) Venkataramanan, L.; Yi-Qiao, S.; Hurlimann, M. D. Solving Fredholm Integrals of the First Kind with Tensor Product Structure in 2 and 2.5 Dimensions. *IEEE Trans. Signal Process.* **2002**, *50*, 1017−1026.
(53) Korb, J. Nuclear Magnetic Relaxation of Liquids in Porous Media. *New J. Phys.* **2011**, *13*, No. 035016.
(54) Zhao, H.; Wang, Y.; Yang, Y.; Shu, X.; Yan, H.; Ran, Q. Effect of Hydrophobic Groups on the Adsorption Conformation of Modified Polycarboxylate Superplasticizer Investigated by Molecular Dynamics Simulation. *Appl. Surf. Sci.* **2017**, *407*, 8−15.
(55) Watson, A. T.; Chang, C. T. P. Characterizing Porous Media with NMR Methods. *Prog. Nucl. Magn. Reson. Spectrosc.* **1997**, *31*, 343−386.
(56) Pop, A.; Badea, C.; Ardelean, I. The Effects of Different Superplasticizers and Water-to-Cement Ratios on the Hydration of Gray Cement Using T_2-NMR. *Appl. Magn. Reson.* **2013**, *44*, 1223−1234.
(57) Muncaci, S.; Mattea, C.; Stapf, S.; Ardelean, I. Frequency-Dependent NMR Relaxation of Liquids Confined inside Porous Media Containing an Increased Amount of Magnetic Impurities. *Magn. Reson. Chem.* **2013**, *51*, 123−128.
(58) Wyrzykowski, M.; Lura, P. The Effect of External Load on Internal Relative Humidity in Concrete. *Cem. Concr. Res.* **2014**, *65*, 58−63.
(59) Wyrzykowski, M.; Lura, P. Rh Dependence Upon Applied Load: Experimental Study on Water Redistribution in the Microstructure at Loading. *Concreep 10* **2015**, 339−347.
(60) Bresson, B.; Meducin, F.; Zanni, H.; Noik, C. Hydration of Tricalcium Silicate (C_3S) at High Temperature and High Pressure. *J. Mater. Sci.* **2002**, *37*, 5355−5365.
(61) Maruyama, I.; Rymeš, J.; Vandamme, M.; Coasne, B. Cavitation of Water in Hardened Cement Paste under Short-Term Desorption Measurements. *Mater. Struct.* **2018**, *51*, No. 159.
(62) Wyrzykowski, M.; Lura, P. Moisture Dependence of Thermal Expansion in Cement-Based Materials at Early Ages. *Cem. Concr. Res.* **2013**, *53*, 25−35.
(63) Radjy, F.; Sellevold, E. J.; Hansen, K. K. *Isosteric Vapor Pressure - Temperature Data for Water Sorption in Hardened Cement Paste: Enthalpy, Entropy and Sorption Isotherms at Different Temperatures*; Technical University of Denmark: Lyngby, 2003.
(64) Jensen, O. M., The Pozzolanic Reaction of Silica Fume. *MRS Online Proc. Libr. Arch.* **2012**, *1488*, DOI: 10.1557/opl.2012.1539.
(65) Geng, G.; Myers, R. J.; Qomi, M. J. A.; Monteiro, P. J. M. Densification of the Interlayer Spacing Governs the Nanomechanical Properties of Calcium-Silicate-Hydrate. *Sci. Rep.* **2017**, *7*, No. 10986.
(66) Holly, R.; Reardon, E. J.; Hansson, C. M.; Peemoeller, H. Proton Spin−Spin Relaxation Study of the Effect of Temperature on White Cement Hydration. *J. Am. Ceram. Soc.* **2007**, *90*, 570−577.

DOI: 10.1021/acs.jpcc.9b02436
J. Phys. Chem. C 2019, 123, 16153−16163